ORIGINALARBEITEN/ORIGINALS

CFD analysis on the oil flow of a gear stage with guide plate

Lucas Hildebrand[1] · Florian Dangl[1] · Martin Sedlmair[1] · Thomas Lohner[1] · Karsten Stahl[1]

Abstract

Gearbox housing geometry and oil guide plates strongly influence gearbox oil flow and interaction of oil with machine elements. Guided oil flow can increase gearbox efficiency and improve heat management. Recent research studies have demonstrated the potential of Computational Fluid Dynamics (CFD) simulations to predict the gearbox oil flow and no-load losses. Thereby, the influence of housing geometry and guide plates has rarely been addressed. This study focuses on a CFD analysis on the oil flow of a dip lubricated spur gear stage with a guide plate. Grid-based CFD models with different simulation setups were confronted and evaluated. Results show that the selection of the simulation setup with respect to the acceleration ramp and mesh size needs to address the considered object of investigation and the desired depth of information. An appropriate simulation setup shows great accordance with recordings of the oil distribution by a high-speed camera. A detailed analysis of the simulation results identified the contribution of different gear surface zones to the no-load gear loss torque. For the considered guide plate a strong interaction of oil flow and loss torque due to pressure forces on the tooth flank surface zones and due to shear forces on the front and tip circle surface zones of the gears was determined.

CFD-Analyse der Ölströmung in einem Getriebe mit Leitblech

Zusammenfassung

Die Geometrie des Getriebegehäuses sowie Ölleitbleche haben einen starken Einfluss auf die Ölströmung in Getrieben und folglich auf die Interaktion von Öl mit Maschinenelementen. Eine geführte Ölströmung kann den Getriebewirkungsgrad steigern und dessen Wärmehaushalt verbessern. Aktuelle Forschungsarbeiten zeigen das Potential der Computational Fluid Dynamics (CFD) zur Vorhersage der Getriebeölströmung sowie auftretender Leerlaufverluste. Hierbei wurde der Einfluss der Gehäusegeometrie oder jener von Leitblechen bisher wenig thematisiert. Diese Studie beschäftigt sich mit der CFD-Analyse der Getriebeölströmung in einem tauchgeschmierten, einstufigen Stirnradgetriebe mit Leitblech. Auf Basis netzbasierter Simulationsmodelle werden verschiedene Simulationssetups gegenübergestellt und bewertet. Die Ergebnisse zeigen, dass bei der Definition wesentlicher Parameter eines Simulationssetups, wie bspw. Netzdichte und Beschleunigungsrampe, der betrachtete Untersuchungsgegenstand sowie die gewünschte Ergebnistiefe zu berücksichtigen sind. Ein geeignetes Simulationssetup ermöglichte eine präzise Vorhersage der Ölverteilung am Prüfstand, welche anhand einer Hochgeschwindigkeitskamera erfasst wurde. Für das betrachtete Leitblech konnte ein starker Einfluss der Getriebeölströmung auf das resultierende Leerlaufverlustmoment festgestellt werden. Auf Basis einer detaillierten Analyse der Simulationsergebnisse konnte der Beitrag verschiedener Zahnradoberflächenbereiche auf das verzahnungsbedingte Leerlaufverlustmoment bewertet werden. Hierbei wurde ein wesentlicher Einfluss der Druckkräfte auf Zahnflankenoberflächen sowie Scherkräfte auf Stirn- und Kopfkreisoberflächenbereiche festgestellt.

✉ Lucas Hildebrand
hildebrand@fzg.mw.tum.de

Florian Dangl
flo.dangl@tum.de

Martin Sedlmair
sedlmair@fzg.tum.de

Thomas Lohner
lohner@fzg.mw.tum.de

Karsten Stahl
stahl@fzg.mw.tum.de

1   Gear Research Centre (FZG), Technical University of Munich (TUM), Boltzmannstraße 15, 85748 Garching near Munich, Germany

1 Introduction

Within the development of modern powertrains, a deep understanding of the system interactions and components is fundamental for optimal design. By means of Computational Fluid Dynamics (CFD) simulations of the oil flow in gearboxes, essential information can be derived at an early stage of the development process, enabling an optimized gearbox design at reduced development costs. For lubrication and heat dissipation within gearboxes, different lubrication methods are available, such as dip or injection lubrication. Dip lubrication is widely used due to its simplicity and low technical effort required for implementation. Oil dip lubrication is mostly used in applications with circumferential speeds below $v_t = 20\,\text{m/s}$. By targeted implementation of oil guide plates, it has been successfully adapted for applications with circumferential speeds up to 60 m/s [15]. Thereby, the guidance of oil flow ensures the sufficient oil supply of machine elements.

The interaction of rotating machine elements with oil results in different effects influencing the gearbox efficiency and heat balance. For gears, the interactions churning, squeezing, impulse, and windage are classified. For dip lubricated gearboxes the interactions churning, squeezing and windage are relevant. Churning describes the displacement of oil due to continuous dipping and rotation of immersed gears in the oil sump. The engagement of gears can result in squeezing of lubricant out of the gear meshing zone. The interaction of rotating gears with a second fluid (mostly air) causes windage effects. Regarding dip lubricated gearboxes, the power losses resulting from churning $P_{LG0,C}$, squeezing $P_{LG0,S}$ and windage $P_{LG0,W}$ add to the no-load gear power loss P_{LG0} [32]:

$$P_{LG0} = P_{LG0,C} + P_{LG0,S} + P_{LG0,W} \tag{1}$$

Numerous research studies point out the influence of the interaction between rotating gears and oil on the no-load gear loss. Mauz [32] performed extensive experimental investigations on the loss behavior of spur gears. Based on his results, a set of empirical equations has been derived by which the no-load gear loss can be determined. Detailed investigations on the windage phenomena for high-speed and injection lubricated gearboxes were carried out by Maurer [31]. Recent experimental studies by Quiban et al. [39] investigated the transition between churning and windage with respect to spur gears. Here, the authors determine a strong interaction of the predominant air flow with the oil sump that influences the power loss of the gearbox. Calculation models have been derived by Changenet et al. [3]. Seetharaman and Kahraman developed calculation models that allow the prediction of churning losses [43] as well as the prediction of squeezing losses [42]. Doleschel [10]

identified the significant influence of oil viscosity and gear immersion depth on the no-load gear loss. Churning introduces air into the oil. The underlying aeration effect was investigated inter alia by Leprince et al. [22] and Neurouth et al. [34].

Besides dedicated research on the influences on no-load gear losses, several studies analyzed technical possibilities to reduce power losses by control of the interaction of rotating gears with oil. Within his studies, Mauz [32] investigated the influence of different guide plate geometries on the oil flow and no-load loss of a spur gearbox. Results show the potential of guide plates to control the oil flow. For some configurations, increased no-load losses were found whereby the interaction of the gearbox fluid flow with the guide plate was assumed to be causal. Otto [37] analyzed the potential of minimized quantity lubrication to increase gearbox efficiency. It is shown that for dip lubricated gearboxes a targeted implementation of a guide plate can control the interaction of rotating gears with oil leading to reduced no-load losses. Leoni [20] describes the potential of a targeted and spatial separated supply of oil for the purposes of lubrication and heat transfer regarding the increase of gearbox efficiency and operational safety. Experimental investigations on the oil distribution of a dip lubricated gearbox were performed by Norgauer et al. [35] and Leprince et al. [21].

The interaction of rotating gears with oil is a complex flow phenomenon. Hence, a deep understanding of the mechanisms is fundamental for optimal gearbox design. CFD simulations of the gearbox oil flow have the potential to derive essential information at an early stage of a gearbox development process (Morhard et al. [33], Concli and Gorla [7]). Maccioni and Concli [28] provide an overview of applied CFD methods and investigations regarding lubrication of machine elements and gearboxes. A large number of numerical studies on the gearbox oil flow and no-load loss are based on the grid-based Finite Volume Method (FVM). However, particle-based CFD methods like the Smoothed Particle Hydrodynamics (SPH) also gain relevance. Within particle-based methods, the fluids are discretized by particles that are attributed with physical quantities to describe the properties and behavior of the fluids. Shadloo et al. [44] provide an overview on the potential of SPH for industrial applications. The great potential of SPH to predict the gearbox oil flow is specifically stated by several workers (Keller et al. [18], Morhard et al. [33]). This is confirmed by Liu et al. [23], but the authors point out significant challenges when predicting no-load gear losses and mechanisms of the interactions between rotating gears and oil precisely.

Regarding the grid-based FVM, several numerical studies focus on the prediction of power loss of gearboxes by means of single-phase simulations. Squeezing effects were

investigated by Concli and Gorla [5]. Numerical investigations on windage phenomena were carried out by Chaari et al. [2], Pallas et al. [38], Concli et al. [8], and Ruzek et al. [40]. The confrontation of simulation results with experimental measurements within [8, 38] and and [40] showed good accordance. Multiphase simulations based on the FVM were applied in numerous studies to investigate the oil flow and the interaction of gears with oil within injection and dip lubricated gearboxes. In terms of injection lubricated gearboxes, investigations were carried out by Fondelli et al. [13], Liu et al. [26] and Keller et al. [19]. Thereby, a strong focus was put on the interaction of rotating gears with the oil jet. Liu et al. [26] also investigated the no-load gear loss behavior, both in a time-dependent manner and depending on the circumferential speed and oil viscosity. Numerical results showed good agreement with results from empirical equations. In terms of dip lubrication, investigations on the oil flow and no-load gear loss behavior were performed by Gorla et al. [17], Concli and Gorla [6], Liu et al. [24, 25], and Mastrone et al. [30]. Within the presented studies, simulated no-load losses were compared with experimental measurements whereby a good accordance is stated. In addition to no-load losses, Liu et al. [25] focus on the resulting oil distribution within the gearbox. The comparison with oil distributions at the corresponding test rig by means of a high-speed camera are in good accordance. Specifically the trajectories of spun oil were predicted accurately. Dip lubricated planetary gearboxes were investigated numerically by Concli et al. [4] and Liu et al. [27]. These works show the potential of the FVM for studying complex gearbox geometries.

Many analyses on the oil flow and no-load loss of dip and injection lubricated gearboxes have been performed. The literature review was focused on the interaction of rotating gears with oil; however the interaction of rotating bearings with oil was also studied in detail e.g. by Feldermann et al. [11], Marchesse et al. [29], and Concli et al. [9]. Thanks to the introduction of the CFD method to gearboxes, the understanding of the oil flow mechanisms has improved significantly. The presented CFD studies show the great potential of FVM regarding the determination and accurate prediction of investigated loss phenomena related to gearboxes. Experimental results on oil guide plates show the potential to control gearbox oil flow, but an increase of power losses was partially found. So far, the oil flow and interaction of gears with oil in gearboxes with guide plates has been poorly understood.

This study aims at extending the understanding of guided multiphase fluid flow in gearboxes and highlights the importance of a needs-based simulation setup. Grid-based CFD simulations with different simulation setups were carried out with focus on the oil flow and no-load gear loss of a dip lubricated single-stage gearbox with an oil guide plate. Different circumferential speeds were considered. High-speed camera recordings were used to validate simulated oil distributions. A detailed numerical analysis on the mechanisms of interaction of rotating gears with oil was carried out to study the contribution of different gear surface zones to the no-load gear loss.

2 Methodology

Within this study, numerical and experimental investigations on a guided multiphase fluid flow in a gearbox were carried out. In the following, the object of investigation is detailed and the developed CFD models are presented. Basic information on the underlying numerical modeling is given. The considered calculation and experimental procedure is presented.

2.1 Object of investigation

The object of investigation was a single-stage FZG test gearbox as used previously by Liu et al. [24, 25]. The test gearbox has a width of 260 mm, a height of 171 mm and

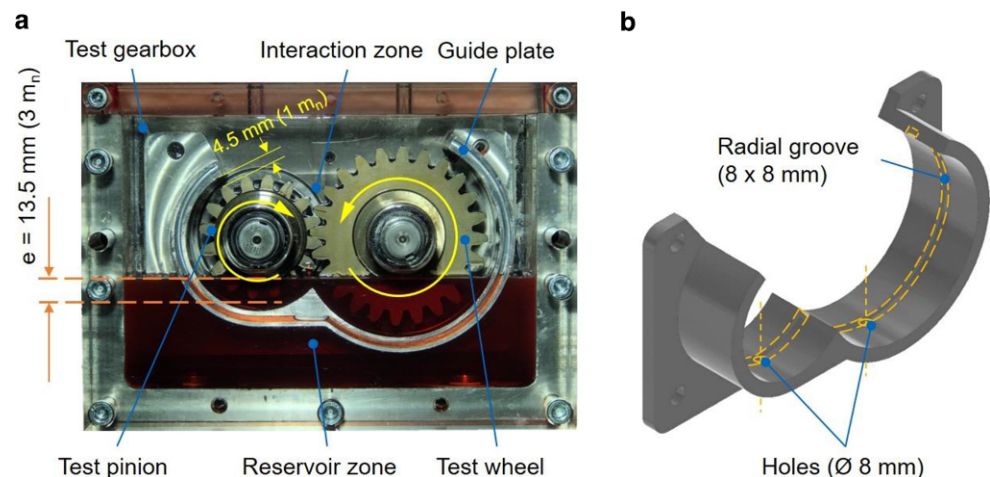Fig. 1 Considered test gearbox with guide plate (a) and CAD model of the guide plate (b)

Table 1 Geometry of the type C-PT gears

	a in mm	$z_{1|2}$	m_n in mm	α_n in °	$x_{1|2}$ in mm	$b_{1|2}$ in mm	$d_{a1|2}$ in mm
Pinion (1)	91.5	16	4.5	20.0	0.182	14	82.5
Wheel (2)		24			0.171		118.4

Table 2 Properties of the considered mineral oil FVA3

Oil	$\rho(15\,°C)$ in kg/m³	$\nu(40\,°C)$ in mm²/s	$\nu(100\,°C)$ in mm²/s	VI Index
FVA3	864	95.0	10.7	95

a depth of 56 mm. The investigated guide plate complies with the one used by Otto [37]. Fig. 1a shows the front view on the test gearbox with the considered guide plate with a radial clearance of 4.5 mm (1 m_n) to the gears. The front cover of the housing is made of acryl glass, enabling the capture of the oil distribution. The guide plate separates the housing in the outer oil reservoir zone and the inner interaction zone where the gears rotate. At the top, the geometry is open so that oil can exit the interaction zone. Fig. 1b pictures the guide plate. Beneath the pinion and wheel, holes with a diameter of 8 mm in the guide plate enable oil to flow through. In radial direction, the guide plate has a rectangular groove with a dimension of 8×8 mm that guides the backflow of oil through the holes.

The considered gears are standard FZG test gears type C-PT [14]. The geometric data for both the pinion and the wheel are listed in Table 1.

2.2 Operating conditions and lubricant

The mineral oil FVA3 with viscosity grade of ISO VG 100 was considered. The surface tension coefficient of FVA3 was measured as 0.0305 N/m by Bobzin et al. [1]. Table 2 gives an overview over the main properties of FVA3.

The considered oil temperature was 40 °C controlled by a temperature sensor placed in the oil sump. The immersion depth regarding the pinion was set to e = 13.5 mm (3 m_n) as indicated in Fig. 1a. To investigate the influence of the circumferential speed, $v_t = \{2.1; 7; 10\}$ m/s were considered. The rotational direction of the gears corresponded to the commonly known designation "W2" by Mauz [32]. This refers to the wheel rotating counterclockwise and the pinion rotating clockwise as indicated in Fig. 1a.

2.3 Numerical model

In the following, the considered numerical models are described and the underlying basics of CFD are presented. The numerical models were implemented and solved in the commercial grid-based CFD software Ansys Fluent 2020/R1 (ANSYS, Inc., Canonsburg, PA, USA). The multiphase flow of oil and air was addressed by means of the Volume of Fluid (VoF) method. A standard k-ε (RNG) turbulence model was applied that is suitable for complex turbulent flows [16, 45]. For detailed information on the fundamentals of Computational Fluid Dynamics the reader is referred to specialist literature [16, 36, 41].

2.3.1 Governing equations

The Navier-Stokes equations describe the conservation of mass and momentum for a fluid flow. The generic conservation equation for a control volume (CV) reads:

$$\frac{\partial}{\partial t}(\rho\Phi) + \underbrace{\Delta(\rho\overline{u}\Phi)}_{F_\Phi} - \underbrace{\nabla\cdot(\Gamma\nabla\Phi)}_{D_\Phi} = q_\Phi \qquad (2)$$

Hereby, the first term on the left side describes the temporal change of a quantity Φ within the CV. Furthermore, F_Φ represents the convective flow and D_Φ the diffusive flow across the boundary of the CV. The last term q_Φ describes the source or sink of the quantity Φ within the CV. The mass and momentum conservation equations consider the following relations:

	Φ	D_Φ	q_Φ
Mass equation	1	0	0
Momentum equation	$\overrightarrow{u}$	$\nabla\cdot\tau$	$-\nabla p + \mu\Delta\overrightarrow{u} + \rho\overrightarrow{g} + \overrightarrow{f}$

The fluid flow is considered isothermally and therefore the energy equation is not taken into account [12]. Within this study, a Newtonian fluid behavior is considered.

2.3.2 Finite Volume Method

Within the Finite Volume Method (FVM), the calculation domain is subdivided into finite CVs. V is the volume of the control volume and S its surface. Equation 3 shows the generic conservation equation for a quantity Φ in its integral form that describes the temporal change of quantity within a CV (term on the left side), the diffusive flux (first term on the right side) and convective flux (second term on the right side) over the surfaces of the CVs.

$$\frac{\partial}{\partial t}\int_V \rho\Phi\,dV =$$
$$\int_S \Gamma\nabla\Phi\cdot\overrightarrow{n}\,dS - \int_S \rho\Phi\overrightarrow{u}\cdot\overrightarrow{n}\,dS + \int_V q_\Phi\,dV \qquad (3)$$

The parameter $\overrightarrow{n}$ represents the unit vector orthogonal to the specific surface and $\overrightarrow{u}$ is the fluid velocity. The discretization results in a system of partial differential equations. Surface and volume integrals can be determined by

suitable quadrature formulas to transfer the partial differential equations (in time and space) into a set of linear equations. The solving process requires the approximation of variable values, based on interpolation between CVs. Hereby, the FVM is conservative due to spatially fixed CVs and the interrelation of CV averages and CV fluxes over the surfaces. The FVM can adopt any type of grid and is therefore suitable for complex geometries.

2.3.3 Volume of Fluid Method

Within practical applications, besides a fluid in liquid phase (e.g., oil) a secondary gaseous phase (e.g., air) is often involved. The operation of gearboxes can result in a strong interaction of rotating components with the multiple phases as well as between the individual phases. In CFD, multiphase flow can be considered by the Volume of Fluid (VoF) method. The VoF method allows solving the transport equations for individual phases i and j within a CV. On this basis, an averaged generic field property Φ for each CV can be determined due to consideration of the volume phase fraction α and the individual field properties Φ_i and Φ_j:

$$\Phi = \Phi_i \alpha + \Phi_j (1 - \alpha) \tag{4}$$

2.3.4 Turbulence model

Gearbox fluid flow appears to be turbulent within usual operating conditions. From a numerical point of view, the consideration of turbulence appears to be complex due to nonlinear correlation terms involving unknown fluctuating variables. Therefore, turbulence models have been developed to consider turbulence by means of simplified mathematical models. Hereby, fluid flow quantities can be described by means of a time-weighted average term and an oscillating term. The oscillating term is determined by transport equations, so that the averaged Navier-Stokes equations can be written in closed form. For CFD simulation of fluid flow in gearboxes, the k-ε turbulence model has proven to be suitable [17, 24].

The k-ε turbulence model, as most turbulence models, describes turbulence by means of a velocity and a length scale, whereby the velocity scale is determined by an equation for the turbulent kinetic energy k. The turbulent diffusion of kinetic energy is described by means of a gradient diffusion assumption. The length scale as well as the dissipation of the turbulence is represented by ε and the underlying equation. Within turbulent flows, a transfer of kinetic energy from the mean flow to the turbulence can be assumed that is mathematically described by the production rate of turbulent kinetic energy. The k-ε turbulence model has been further complemented by renormalization operations (renormalization group, RNG) for enhanced performance regarding the modeling of complex turbulent flow [45].

2.3.5 Geometry and mesh

Mesh models of the considered test gearbox with guide plate (see Fig. 1) were developed based on experience and previous studies with FVM by Liu et al. [24–26]. The modeling of the transient gear mesh requires an adapted dynamic mesh handling technique, as the mesh is distorted due to the rotation and engagement of gears. The local remeshing method is used, whereby the mesh is locally renewed when a certain distortion is exceeded. The mesh distortion is evaluated with respect to the length and skewness of mesh elements. As the considered test gearbox is characterized by a symmetry in z-direction (see Fig. 2), a half model was used. Thereby, the meshing and calculation effort was reduced by a 2.5D meshing approach. Due to the meshing of the gears, the gears were scaled to 98% of their actual size. The scaling ensured a gap between the tooth flanks that enables the reliable discretization by the considered element sizes within numerical calculation [24]. Pre-investigations have shown a relatively small influence of this scaling on the quality of results regarding oil distribution and simulated no-load gear loss torque for the operating conditions considered. In oil lubricated gearboxes, generally a distinct gearbox fluid distribution develops with increasing circumferential speed of gears [24]. In terms of FVM simulations, the size of the finite volumes determines the possible resolution of the flow field. A finer mesh can help to resolve the predominant flow field more precisely. Preliminary experimental investigations with the considered
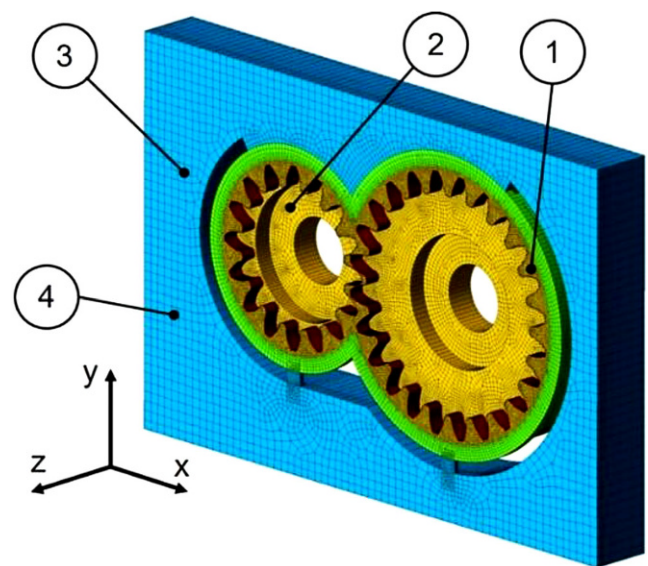

Fig. 2 Mesh model of the considered test gearbox (Mesh$_{0.35M\text{-gIrem}}$)

Table 3 Properties of the considered mesh models

Mesh Zone	$Mesh_{0.35M\text{-}gIrem}$			$Mesh_{1.5M\text{-}gIrem}$		
	Element size in mm	Element number	Density in elements per mm^3	Element size in mm	Element number	Density in elements per mm^3
(1) Remeshing zone	1.00	162,336	1.7	0.75	376,990	3.9
(2) Inner zone	2.00	109,204	0.5	0.75	429,499	2.0
(3) Transition zone	2.00	35,139	0.5	1.00	120,776	1.7
(4) Outer zone	4.00	39,732	0.1	1.00	650,184	1.0
Overall (weighted)	1.76	346,409	0.3	0.87	1,577,449	1.5

Fig. 3 Consecutive simulation methodology for $Setup_{0.35M\text{-}gIrem}$ (**a**) and for $Setup_{1.5M\text{-}gIrem}$ (**b**)
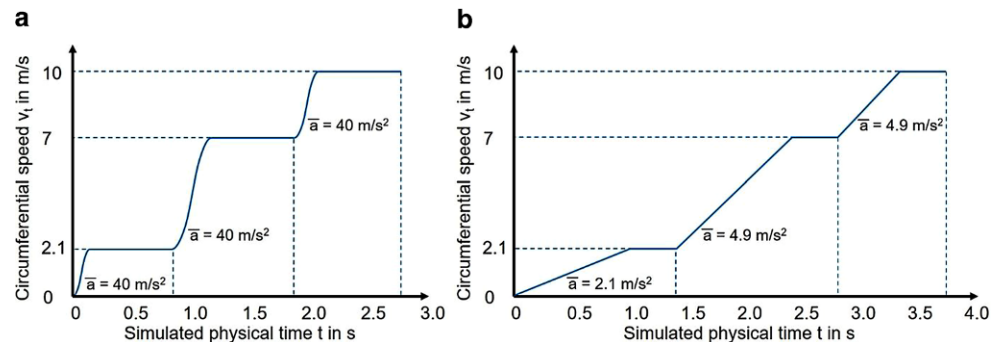
guide plate showed pronounced interaction of rotating gears with oil within the interaction zone. No distinct oil flow in the reservoir zone was observed. Therefore, graded mesh models with element sizes related to the observed predominant flow characteristics were considered. Two graded mesh models were developed to investigate the fluid flow within the gearbox with guide plate. The structure of the mesh exemplarily shown in Fig. 2 is the same for both considered mesh models.

The remeshing zone (1) consists of prismatic cells. The inner zone (2) as well as transition zone (3) and the outer zone (4) are meshed with hexaedric cells. The transition zone (3) connects the remeshing and outer zone. Table 3 gives relevant information on the mesh models. The mesh model $Mesh_{1.5M\text{-}gIrem}$ has an element number of about 1.5 M that is about four times higher than the element number of $Mesh_{0.35M\text{-}gIrem}$ with 0.35 M. The number in the mesh model abbreviation indicates the overall element number. The coarse mesh model $Mesh_{0.35M\text{-}gIrem}$ allows contrasting the computational cost and accuracy. The very fine mesh model $Mesh_{1.5M\text{-}gIrem}$ is used for detailed investigations on the interaction of rotating gears with fluid flow.

The no-load gear loss torque results from the interaction between rotating gears and fluid. For numerical evaluation, pressure and shear forces on the gear surfaces are integrated over each finite volume related to the individual gear surface and multiplied with the corresponding distance to the rotation axis center. Therefore, loss torque portions resulting from the interaction modes churning, squeezing, and ventilation are generally included in the simulated no-load gear loss torque $T_{L0,sim}$.

2.4 Calculation procedure

In the following, the calculation procedures for the performed numerical investigations are presented. As the CFD simulation starts from an initial motionless state, an acceleration ramp is required to ensure numerical stability and to relate to physical circumstances in technical applications. After passing through the acceleration ramp, a certain physical time is calculated to enable a quasi-stationary simulation state (see Sect. 3.2). The quasi-stationary state of a simulation also defines the starting point for the simulation of a higher circumferential speed within a consecutive simulation methodology.

The mesh models of Sect. 2.3.5 were used to investigate the gearbox fluid flow and were incorporated into the individual simulation setups $Setup_{0.35M\text{-}gIrem}$ and $Setup_{1.5M\text{-}gIrem}$. The simulation setup $Setup_{0.35M\text{-}gIrem}$ took the approach of minimized calculation costs. Besides the relatively coarse mesh model, an acceleration ramp with a mean acceleration value of $\bar{a} = 40 \text{ m/s}^2$ was used. Hereby the numerical stability of the simulations was supported by sinusoidal acceleration ramps.

The simulation $Setup_{1.5M\text{-}gIrem}$ was configured to investigate potential increase of predictive accuracy. Therefore, linear acceleration ramps were set. The physical acceleration time of $t_a = 1 \text{ s}$ was applied for $v_t = \{2.1; 7\}$ m/s. For the consecutive simulation to $v_t = 10 \text{ m/s}$ the same acceleration value of the previous simulation ($v_t = 7 \text{ m/s}$) was used, resulting in the acceleration time $t_a = 0.6 \text{ s}$. For simulations based on $Setup_{1.5M\text{-}gIrem}$, after terminating the acceleration phase, less time was needed to be calculated due to a faster

Table 4 Considered acceleration ramps and investigated physical simulation times for $\text{Setup}_{0.35\text{M-gIrem}}$ and $\text{Setup}_{1.5\text{M-gIrem}}$

v_t in m/s	$\text{Setup}_{0.35\text{M-gIrem}}$			$\text{Setup}_{1.5\text{M-gIrem}}$		
	$\overline{a}$ in m/s^2	t_a in s	t_{tot} in s	$\overline{a}$ in m/s^2	t_a in s	t_{tot} in s
2.1	40.0	0.053	0.80	2.1	1.00	1.40
7	40.0	0.123	1.15	4.9	1.00	1.40
10	40.0	0.075	0.75	4.9	0.60	1.00

forming quasi-stationary state compared to $\text{Setup}_{0.35\text{M-gIrem}}$. The circumferential speed over time for consecutive simulations is shown in Fig. 3a for $\text{Setup}_{0.35\text{M-gIrem}}$ and in Fig. 3b for $\text{Setup}_{1.5\text{M-gIrem}}$.

In Table 4 details of the simulation setups based on Table 3 are presented. Hereby, the mean acceleration value $\overline{a}$ used during the acceleration ramp, the acceleration time t_a, and the quasi-stationary simulation time t_{tot} are listed.

In accordance with previous studies [24, 25], a time step was chosen that results in a change of rotation angle of the pinion of 0.1°. This time step ensures a stable remeshing process. The corresponding Courant-Friedrich-Lewy numbers are approximately 0.1. A local convergence criterion of 10^{-5} was defined in the solving process and used for all equations. The calculations were carried out at the Leibnitz Rechenzentrum (LRZ). Regarding the calculation resources, 112 cores (Intel Xeon E5-2690 v3 @ 2.6 GHz) and 64 Gb Ram were used. The simulations were carried out with the software Ansys Fluent (Release 2020 R1). The required calculation time for the simulation of one pinion rotation averaged out to approximately 2.5 h for $\text{Setup}_{0.35\text{M-gIrem}}$ and 8 h for $\text{Setup}_{1.5\text{M-gIrem}}$.

2.5 Experimental procedure

The test gearbox in Fig. 1 was experimentally investigated at the FZG no-load power loss test rig. This test rig was also used in previous studies [24, 25], which the following description is partly based on. The mechanical layout is shown in Fig. 4. The electric engine drives the intermediate gearbox that is connected with the test gearbox. The adaption of a loss torque meter ahead of the test gearbox enables the measurement of the no-load loss of the test gearbox. The no-load loss of the gearbox includes the losses from the gears, the bearings, and the ones from the rotary shaft seals. Specific gear-based no-load losses can be extracted by additional investigations to determine the no-load losses from bearings and sealings [8]. The considered torque meter has a measuring range of 10 Nm and an uncertainty in measurement of ±0.1%. The transparent front cover of the test gearbox (see Fig. 1) enables capturing the oil distribution within the test gearbox during operation.

Quasi-stationary oil distributions were captured for all investigated circumferential speeds $v_t = \{2.1; 7; 10\}$ m/s by
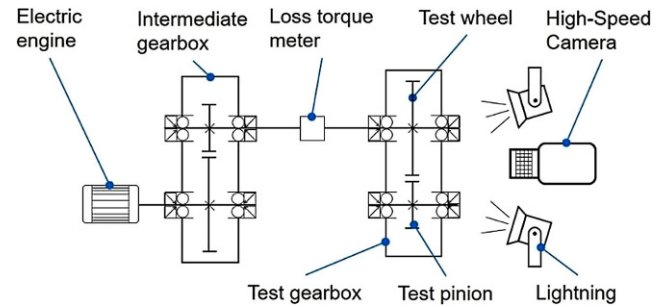

Fig. 4 Mechanical layout of the FZG no-load power loss test rig

means of a high-speed camera running at 3000 fps. Before each test, the test rig was set up corresponding to the defined operating conditions (see Sect. 2.2). The oil was colored red by means of a special dye to increase contrast. As relatively small circumferential speeds were being considered, no-load loss torques were expected to be small and difficult to evaluate with sufficient resolution. Hence, it was not evaluated.

3 Results and discussion

Based on the described methodology, numerical calculations were performed. The results are analyzed and discussed in the following.

3.1 Oil distribution

The simulated oil distributions are evaluated at maximum physical time t_{tot} simulated per circumferential speed (see Table 4). Regarding the front views on the oil distribution, the oil fraction within the circumferential groove and the holes in the guide plate is pictured in the view plane. Fig. 5 shows the frontal and isometric view on the simulated oil distributions for $v_t = \{2.1; 7; 10\}$ m/s based on the $\text{Setup}_{0.35\text{M-gIrem}}$. It can be seen that the guide plate prevents oil from being spun off the gears directly in radial direction and guides the oil in circumferential direction. Consequently, within the interaction zone, oil is dragged and an oil circulation can be identified, resulting in an interaction of gears with oil. The focus on $v_t = 2.1$ m/s shows that an oil sump is present on the bottom of the interaction zone. An oil flow caused by the gear wheel is impinging on the pinion. It can be observed during the acceleration phase, that oil is spun out of the interaction zone to the outer reservoir zone.

For the higher circumferential speeds $v_t = \{7; 10\}$ m/s an increased amount of oil is spun out into the outer reservoir zone due to the longer lasting acceleration ramps; therefore, an increased oil level in the reservoir zone can be determined. As a result, the interaction of gears with oil

Fig. 5 Simulated oil distribution in frontal and isometric view visualized by oil fraction for $v_t = \{2.1; 7; 10\}$ m/s based on the Setup$_{0.35M\text{-gIrem}}$
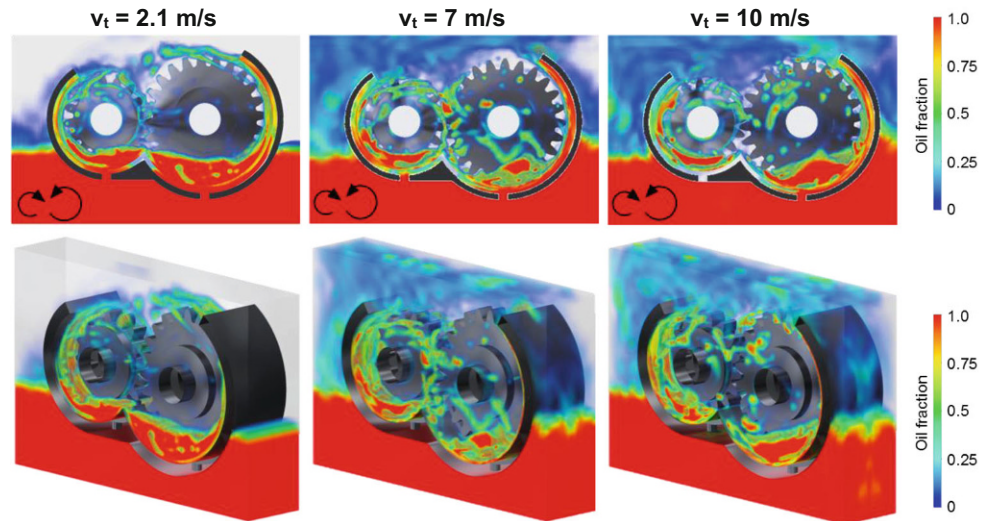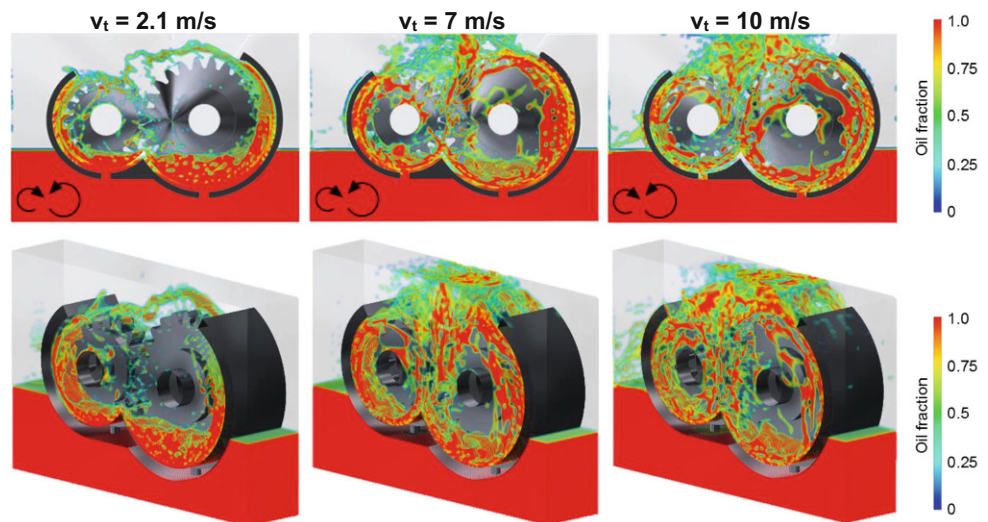

Fig. 6 Simulated oil distribution in frontal and isometric view visualized by oil fraction for $v_t = \{2.1; 7; 10\}$ m/s based on the Setup$_{1.5M\text{-gIrem}}$

within the guide plate geometry is reduced. The oil fractions that are spun out of the guide plate geometry are present as a homogenized and diffuse fluid mixture. No defined fluid pattern can be identified in the outer region. The focus on the groove and on the hole beneath the pinion shows that with increasing circumferential speed the oil fraction directly underneath the gear engagement area is reduced. Here it can be assumed that the predominant air flow causes the displacement of oil in circumferential direction.

Fig. 6 shows corresponding to Fig. 5 the simulated oil distributions for $v_t = \{2.1; 7; 10\}$ m/s based on the Setup$_{1.5M\text{-gIrem}}$. In comparison with Fig. 5, a more detailed oil flow pattern due to the higher mesh density can be stated for Setup$_{1.5M\text{-gIrem}}$. For $v_t = 2.1$ m/s the simulation results based on Setup$_{0.35M\text{-gIrem}}$ and Setup$_{1.5M\text{-gIrem}}$ show qualitatively good accordance. An oil flow caused by the gear wheel impinging on the pinion is predicted by both simulation setups.

However, remarkably different oil distributions are found in the outer reservoir zone and particularly for the higher circumferential speeds. This is mainly due to the much slower acceleration ramps for Setup$_{1.5M\text{-gIrem}}$, so that less oil is spun out of the interaction zone to the outer reservoir zone during the acceleration phase. Hence, no significant change of the oil level in the outer reservoir zone is observed for the investigated circumferential speeds. For $v_t = \{7; 10\}$ m/s, an oil flow is directed to the top of the housing. Thereby, the oil is not spun out to the outer reservoir zone but flows back downwards into the interaction zone. This results in a strong interaction of the rotating gears with oil and the fluid flows caused by the pinion and wheel, which are also strongly interacting.

For the circumferential speeds $v_t = \{7; 10\}$ m/s it can be observed, that contrary to $v_t = 2.1$ m/s the oil flow caused by the gear wheel is directed more to the top of the housing and the oil flow caused by the pinion is impinging on the

gear wheel. The focus on the isometric view shows, that for $v_t = \{7; 10\}$ m/s, a displacement of oil in axial direction is predominant and oil is wetting the front cover as well as impinging on the shafts. The focus on the groove within the guide plate shows that with increasing circumferential speeds, the oil fraction directly underneath the gear engagement area is reduced.

It can be stated that both simulation setups predict a comparable behavior of the predominant oil flow. However, the simulations based on Setup$_{1.5M\text{-}gIrem}$ predict a stronger interaction of rotating gears with oil compared to Setup$_{0.35M\text{-}gIrem}$ mainly due to the slower acceleration ramp.

In the following, simulation results based on Setup$_{1.5M\text{-}gIrem}$ are compared with experimental results. Fig. 7 compares the simulated oil distributions with oil distributions captured by the high-speed camera at the FZG no-load power loss test rig (see Sect. 2.5). The analysis of the recorded oil distributions verifies that no considerable change of the oil level of the outer reservoir zone is predominant for the investigated speeds.

For $v_t = 2.1$ m/s, a distinct oil flow caused by the gear wheel impinging on the pinion is observable. Regarding the higher speeds $v_t = \{7; 10\}$ m/s, an oil flow directed to the top of the gearbox housing is predominant and an oil flow caused by the pinion impinging on the gear wheel can be identified. An allocation of the oil sump within the interaction zone due to circulation of oil can be stated. In addition,

it can be seen that oil is displaced in axial direction wetting the front cover and interacting with the shafts. The focus on the guide plate geometry underneath the gear engagement shows that with increased circumferential speed, more oil is displaced. This could be caused by an introduced air flow induced by the rotating gears. In general, the comparison of recorded and simulated oil distributions shows a good accordance.

Based on the analysis of simulation results and comparison with experimental data, it can be stated, that the mechanisms of the gearbox oil flow are presented well for the simulation setup Setup$_{1.5M\text{-}gIrem}$. For Setup$_{0.35M\text{-}gIrem}$, the acceleration ramp is too harsh; the oil is spun out to the outer reservoir zone. Hence, besides the coarse resolution, the interaction of rotating gears with oil cannot be realistically predicted within the simulated physical time. In contrast, the Setup$_{1.5M\text{-}gIrem}$ shows a realistic flow pattern and local oil fractions due to the finer mesh.

3.2 No-load gear loss

The simulated oil distributions shown in Sect. 3.1 are linked to the emerging no-load gear loss torques. Fig. 8a shows the simulated no-load gear loss torque $T_{L0,sim}$ for $v_t = 2.1$ m/s based on the Setup$_{0.35M\text{-}gIrem}$. During the acceleration phase, a torque maximum is predominant due to the previously described impingement of oil on the wheel (Sect. 3.1) and

Fig. 7 Comparison of measured and simulated (Setup$_{1.5M\text{-}gIrem}$) oil distributions for $v_t = \{2.1; 7; 10\}$ m/s
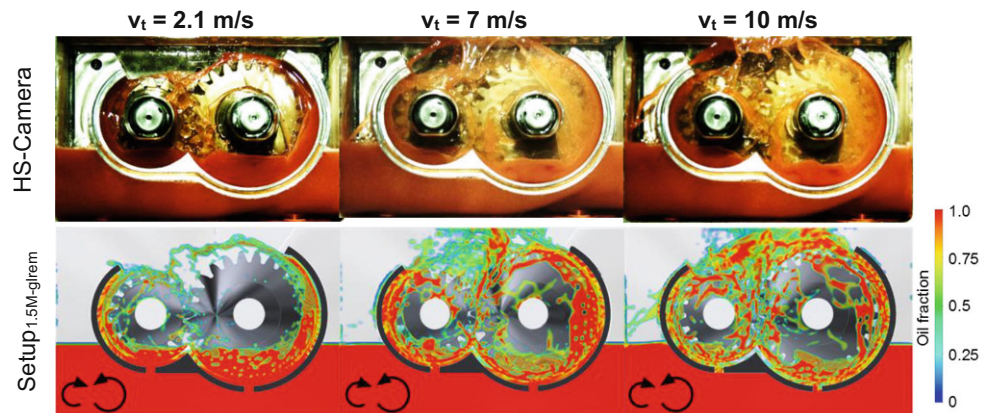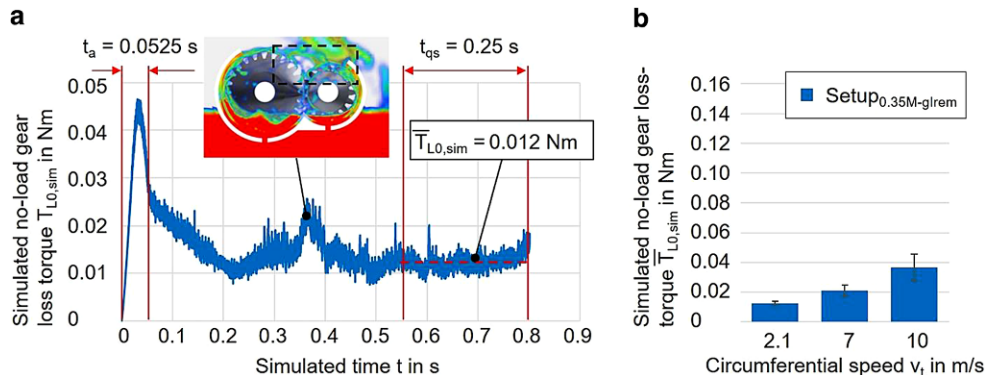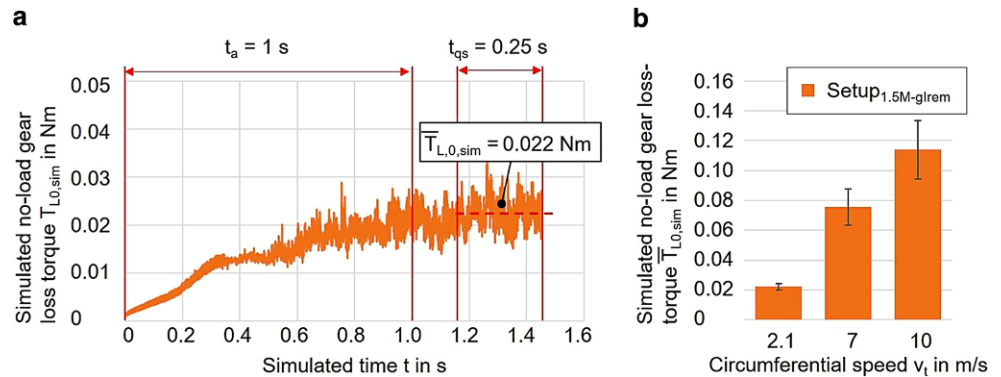

Fig. 8 Simulated no-load gear loss torque over time for $v_t = 2.1$ m/s (**a**) and averaged values over $t_{qs} = 0.25$ s for $v_t = \{2.1; 7; 10\}$ m/s based on Setup$_{0.35M\text{-}gIrem}$ (**b**)

Fig. 9 Simulated no-load gear loss torque over time for $v_t = 2.1$ m/s (**a**) and averaged values over $t_{qs} = 0.25$ s for $v_t = \{2.1; 7; 10\}$ m/s based on Setup $_{1.5M\text{-}gIrem}$ (**b**)

resulting impulse effects. $T_{L0,sim}$ is then strongly related to the oil distribution. At $t = 0.37$ s, the impingement of an oil flow induced by the wheel on the pinion results in a local maximum in $T_{L0,sim}$. The further analysis of the trend of $T_{L0,sim}$ shows that a quasi-stationary state is forming. This allows the determination of a simulated average no-load gear loss torque $\overline{T}_{L0,sim}$. For all investigated speeds the averaging is performed over the time span of $t_{qs} = 0.25$ s physical time. Hereby t_{qs} is related to the quasi-stationary state at the end of each simulation. For the exemplary trend of $T_{L0,sim}$ shown in Fig. 8a, an averaged no-load loss torque of $\overline{T}_{L0,sim} = 0.012$ Nm is derived. Fig. 8b shows $\overline{T}_{L0,sim}$ for $v_t = \{2.1; 7; 10\}$ m/s based on the Setup $_{0.35M\text{-}gIrem}$ complemented with the standard deviation emerging from the fluctuation of the underlying simulated no-load gear loss torque $T_{L0,sim}$. The results show moderately increasing loss torques with increasing circumferential speed.

Fig. 9a shows the simulated no-load gear loss torque $T_{L0,sim}$ for $v_t = 2.1$ m/s based on the Setup $_{1.5M\text{-}gIrem}$. Due to the slower acceleration ramp, a much flatter path of $T_{L0,sim}$ compared to Setup $_{0.35M\text{-}gIrem}$ is observed and no distinct maxima as in Fig. 8a are present. Fig. 9b shows the averaged simulated no-load gear loss torques $\overline{T}_{L0,sim}$ for $v_t = \{2.1; 7; 10\}$ m/s based on the Setup $_{1.5M\text{-}gIrem}$ with an averaging over $t_{qs} = 0.25$ s. The values of $\overline{T}_{L0,sim}$ are remarkably higher compared to those predicted by Setup $_{0.35M\text{-}gIrem}$. As shown in Sect. 3.1, less oil is spun out of the interaction zone for Setup $_{1.5M\text{-}gIrem}$ and consequently a stronger interaction of the gears with the oil is predominant, which results in higher loss torques. The results show increasing loss torques over circumferential speed. The comparison with Fig. 8b shows a significant increase of $\overline{T}_{L0,sim}$ between $v_t = 2.1$ m/s and $v_t = 7$ m/s for Setup $_{1.5M\text{-}gIrem}$. The standard deviation of $\overline{T}_{L0,sim}$ in Fig. 9b based on the Setup $_{1.5M\text{-}gIrem}$ reflects the strong interaction of rotating gears with the oil in the interaction zone.

The analysis of the presented results shows that within Setup $_{0.35M\text{-}gIrem}$, the harsh acceleration ramp results in unrealistic oil distributions and strongly affected oil flows. The predicted quasi-stationary state shows clear differences compared with corresponding experimental measurements. For simulations based on Setup $_{1.5M\text{-}gIrem}$ a quasi-stationary state can be observed subsequent to the acceleration phase. Compared with the experimental measurements, the oil distribution is predicted accurately. It can be assumed that the calculation efficiency within Setup $_{1.5M\text{-}gIrem}$ could be increased by the implementation of suitable faster acceleration ramps. The findings show that customized acceleration ramps depending on the technical application are fundamental for effective and efficient simulations.

3.3 Details on interaction of oil with rotating gears

In the previous sections, promising results based on Setup $_{1.5M\text{-}gIrem}$ have been presented that are in good accordance with recorded oil distributions at the test rig. The simulation results enable a deep analysis of effects and mechanisms related to gearbox oil flow. Therefore, the shell surfaces of the gears are separated in different surface zones. Fig. 10a exemplarily shows the defined surface zones by means of the gear wheel. Thereby, the surface zones of the tip circle, the tooth flanks, the tooth fillets, the fronts, and the shafts are considered.

Fig. 10b shows the evaluated loss proportions across the defined gear surface zones for $v_t = \{2.1; 7; 10\}$ m/s based on Setup $_{1.5M\text{-}gIrem}$. The contribution of the tooth flank surface zones to the overall no-load gear loss torque mainly emerges from pressure forces and amounts to about 40 to 45%. The other surface zones mainly contribute to the overall no-load gear loss torque due to shear forces. Thereby, the front and tip circle surface zones account for a share of about 55 to 60% of the overall no-load gear loss torque. The results also show an increasing proportion of the tooth flank surface zones with increasing circumferential speed. In comparison, the proportions of the tip circle surface zones and tooth fillet surface zones appear to be almost constant within the investigated circumferential speeds. The proportion of the shaft surface zones increases over speed.

Fig. 10b shows for the considered dip lubricated test gearbox with the guide plate a significant influence of shear

Fig. 10 Defined gear surface zones (**a**) and simulated no-load gear loss proportions based on Setup$_{1.5M\text{-gIrem}}$ (**b**)
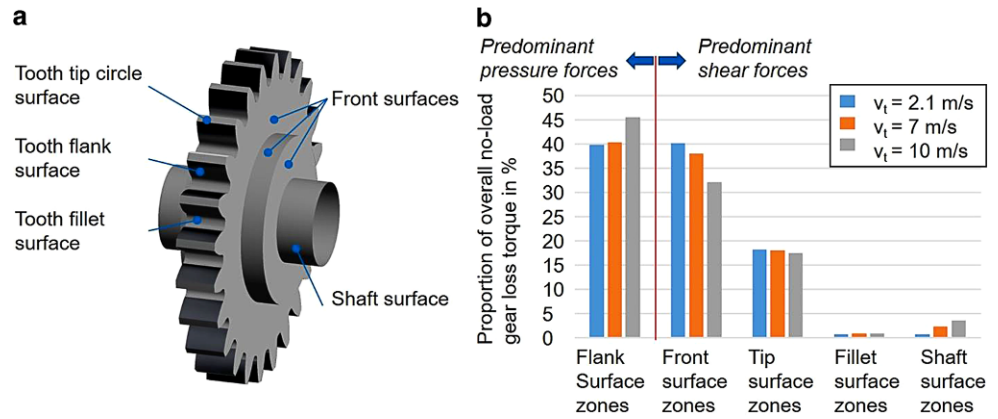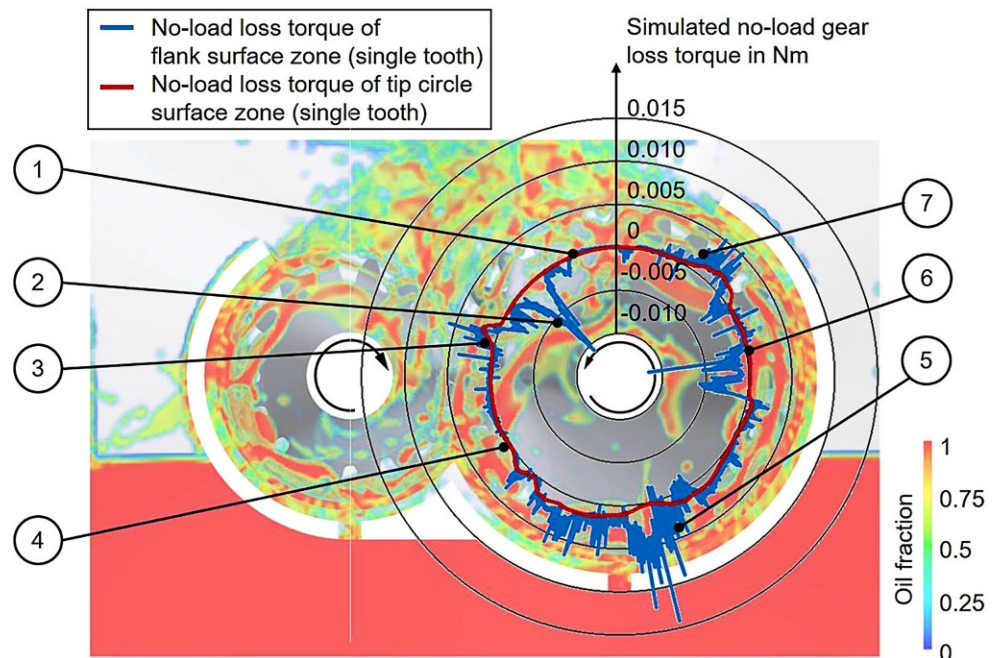

Fig. 11 Simulated no-load loss torque originating from the tooth flank and tooth tip circle surface zone of a single tooth over one rotation of the gear wheel for $v_t = 10$ m/s based on Setup$_{1.5M\text{-gIrem}}$

effects on the no-load gear loss torque. In Liu et al. [24], co-workers of this study investigated the same test gearbox as in this study (see Sect. 2.1) without guide plate under comparable operating conditions. The results from [24] were analyzed regarding the loss torque proportions of the surface zones defined in Fig. 10a. The results show no-load gear loss proportions of the tooth flank surface zones of about 70 to 80% due to pressure forces. This higher proportion of pressure forces can be traced back to a strong interaction of the gears with the oil sump of the gearbox without the guide plate. Hereby, the oil sump is characterized by relatively slow flow speeds compared to the circumferential speed of the gears. In contrast, the oil distribution in this study (see Sect. 3.1) showed a distinctive circulation of oil within the guide plate. Consequently, pressure forces on the tooth flank surface zones are reduced and shear forces become more relevant. In [24], the simulated no-load gear

loss torque for $v_t = 10$ m/s was $\overline{T}_{L0,sim} = 0.14$ Nm. For even deeper understanding of the relation of gearbox oil flow and no-load gear loss torque, a detailed analysis of a single tooth was carried out based on Setup$_{1.5M\text{-gIrem}}$. Thereby, the pressure and shear forces on the flank and tip circle surface zone of one tooth were analyzed for one exemplary rotation at $v_t = 10$ m/s. The corresponding considered time span was between $t = 3.51$ and $t = 3.54$ s (see Fig. 3b). Fig. 11 shows the trend of the no-load gear loss torque originating from the tooth flank surface zone and tip circle surface zone. The corresponding torque center is the rotation axis of the gear wheel.

The considered no-load loss torque portions follow a discontinuous pattern, whereby peaks can be assigned when the tooth accelerates oil, so that pressure forces act on the tooth flanks. In contrast, the considered loss torque due to the tooth tip circle surface zone shows a smoother path. The

Table 5 Phases of interaction of rotating gear tooth with oil based on Fig. 11

Phase	Description
1	Oil is spun off from the wheel, weak interaction of the tooth with oil
2	Impingement of the oil flow caused by the pinion on the wheel, effect of driven tooth and temporary negative torque signal
3	Engagement of gears, squeezing of oil out of the gear meshing zone
4	Displaced oil suspected due to air flow, weak interaction of the tooth with oil
5	High oil fraction and strong interaction of the tooth with oil, strong shear effects on the tooth tip circle surface zone
6	Interaction with turbulent oil flow characterized by temporarily altering torque signal, strong shear effects on tooth tip circle surface zone
7	Accumulation of oil between gears and upper cover of the gearbox housing and strong interaction of the tooth with oil

following phases shown in Table 5 regarding the interaction of the tooth with the oil over the rotation can be identified:

Based on the detailed analysis it can be derived that a strong interaction of the oil flow with the tooth flank surface zones results mainly due to local acceleration of oil impinging on the flanks. This results in pronounced pressure forces (Phases 2, 5–7). In addition, pressure forces are predominant during gear engagement (Phase 3). Hereby, the acceleration of impinging oil is especially noticeable (Phase 2). The interaction of the oil flow with the tooth tip circle surface zones is predominantly based on shear effects. It can be seen that the interaction of a tooth tip circle surface zone with oil is significant during the phase of rotation within the guide plate when passing through an area with high oil volume fraction (Phases 5, 6).

4 Conclusion

Within this study, the oil flow in a dip lubricated single-stage spur gearbox with guide plate was studied by means of the finite volume based CFD method. The appropriate selection of an acceleration ramp in the simulation setup was significant for numerical stability and realistic simulation results. The fine mesh model predicted local oil fractions well and showed great accordance with high-speed camera recordings. The guide plate separates the flow zone within the gearbox housing in a reservoir zone and an interaction zone. A strong relation between predominant oil distribution and emerging no-load gear loss torque was found. A detailed analysis of simulation results identified the contribution of different gear surface zones to the no-load gear loss torque. A strong interaction of oil flow and loss torque due to pressure forces on the tooth flank surface zones was

Table 6 Nomenclature

Symbol	Description	Unit
a	Center distance	mm
$\overline{a}$	Mean acceleration	m/s^2
b	Tooth width	mm
d_a	Tip diameter	mm
e	Immersion depth	mm
D_Φ	Diffusive flow	–
F_Φ	Convective flow	–
m_n	Normal module	mm
P_{LG0}	No-load power loss	W
q_Φ	Source or sink of Φ	–
S	Surface	m^2
t	Time	s
$T_{L0,sim}$	Simulated no-load gear loss torque	Nm
$\overline{T}_{L0,sim}$	Averaged simulated no-load gear loss torque	Nm
V	Volume	m^3
v_t	Circumferential speed	m/s
x	Addendum modification	mm
z	Tooth number	–
α	Volume phase fraction	–
α_n	Pressure angle	°
Γ	Diffusion coefficient	–
μ	Dynamic viscosity	Ns/m^2
ν	Kinematic viscosity	mm^2/s
ρ	Density	kg/m^3
Φ	Generic quantity	–
Vector		
$\overrightarrow{f}$	Forces	*N*
$\overrightarrow{g}$	Gravity	*N*
$\overrightarrow{n}$	Vector orthogonal to surface	–
$\overrightarrow{u}$	Fluid velocity	m/s
Tensor		
τ	Shear stress tensor	N/m^2
Indice		
a	Acceleration	–
C	Churning	–
CV	Control Volume	–
i, j	Phases	–
qs	Quasi-stationary	–
S	Squeezing	–
tot	Total	–
W	Windage	–
1	Pinion	–
2	Wheel	–

determined, e.g., when oil impinges on tooth flank and is accelerated. For the investigated oil guide plate, shear forces on the front and tooth tip circle surface zones of the gears were also found to be a relevant contributor to the no-load gear loss torque. Therefore, the mechanisms of loss emergence regarding the guided oil flow were found to differ from a non-guided oil flow.

5 Nomenclature

The nomenclature is shown in Table 6.

Conflict of interest L. Hildebrand, F. Dangl, M. Sedlmair, T. Lohner and K. Stahl declare that they have no competing interests.

References

1. Bobzin K, Brögelmann T, Kalscheuer C, Thiex M, Ebner M, Lohner T, Stahl K (2018) A contribution to the thermal effects of DLC coatings on fluid friction in EHL contacts. Lubr Sci 30(6):285–299

2. Chaari F, Romdhane MB, Baccar W, Fakhfakh T, Haddar M (2012) Windage power loss in spur gear sets. WSEAS Trans Appl Theor Mech 7:159–168

3. Changenet C, Leprince G, Ville F, Velex P (2011) A note on flow regimes and churning loss modeling. J Mech Des 133(12):13

4. Concli F (2017) Numerical modelling of the churning power losses of gears: an innovative 3D computational tool suitable for planetary gearbox simulation

5. Concli F, Gorla C (2014) A CFD analysis of the oil squeezing power losses of a gear pair. Int J CMEM 2(2):157–167

6. Concli F, Gorla C (2016) Numerical modeling of the power losses in geared transmissions—Windage, churning and cavitation simu-

7. Concli F, Gorla C (2016) Windage, churning and pocketing power losses of gears: different modeling approaches for different goals. Forsch Ingenieurwes 80(3–4):85–99

8. Concli F, Gorla C, Della Torre A, Montenegro G (2014) Windage power losses of ordinary gears: different CFD approaches aimed to the reduction of the computational effort. Lubricants 2(4):162–176

9. Concli F, Schaefer CT, Bohnert C (2020) Innovative meshing strategies for bearing lubrication simulations. Lubricants 8(4):46

10. Doleschel A (2003) Wirkungsgradberechnung von Zahnradgetrieben in Abhängigkeit vom Schmierstoff. Dissertation, Technische Universität München, München

11. Feldermann A, Fischer D, Neumann S, Jacobs G (2017) Determination of hydraulic losses in radial cylindrical roller bearings using CFD simulations. Tribol Int 113:245–251

12. Ferziger JH, Perić M, Street RL (2020) Computational methods for fluid dynamics. Springer, Cham

13. Fondelli T, Andreini A, Da Soghe R, Facchini B, Cipolla L (2015) Numerical simulation of oil jet lubrication for high speed gears. Int J Aerosp Eng 2015(3):1–13

14. Forschungsvereinigung Antriebstechnik e. V. (2010) Einfluss des Schmierstoffes auf die Grübchenlebensdauer einsatzgehärteter Zahnräder im Einstufen- und Lastkollektivversuch. Informationsblatt zum Forschungsvorhaben, vol 2/IV

15. Fritz H (1986) Tauchschmierung – Abschlussbericht – Untersuchungen zur Tauchschmierung von schnelllaufenden Stirnrädern. In: FVA-Nr. 44/IV – Heft 237

16. Gersten K (1981) Einführung in die Strömungsmechanik

17. Gorla C, Concli F, Stahl K, Höhn B-R, Michaelis K, Schultheiss H, Stemplinger J-P (2012) CFD simulations of splash losses of a gearbox. Adcances Tribol. https://doi.org/10.1155/2012/616923

18. Keller MC, Braun S, Wieth L, Chaussonnet G, Dauch T, Koch R, Höfler C, Bauer H-J (2016) Numerical modeling of oil-jet lubrication for spur gears using smoothed particle hydrodynamics. In: 11th International SPHERIC Workshop, Munich, Germany, 13th–16th June 2016

19. Keller MC, Kromer C, Cordes L, Schwitzke C, Bauer H-J (2020) CFD study of oil-jet gear interaction flow phenomena in spur gears. Aeronaut J 124(1279):1301–1317

20. Leoni P (1991) Hochleistungsgetriebe mit getrennter Schmierung und Kühlung. Zugl.: Stuttgart, Univ., Diss., 1991. Inst. für Maschinenkonstruktion u. Getriebebau, Stuttgart

21. Leprince G, Changenet C, Ville F, Velex P (2012) Investigations on oil flow rates projected on the casing walls by splashed lubricated gears. Adv Tribol 2012(5):1–7

22. Leprince G, Changenet C, Ville F, Velex P, Jarnias F (2009) Influence of oil aeration on churning losses. In: The Proceedings of the JSME international conference on motion and power transmissions, p 463–468. https://doi.org/10.1299/jsmeimpt.2009.463

23. Liu H, Arfaoui G, Stanic M, Montigny L, Jurkschat T, Lohner T, Stahl K (2019) Numerical modelling of oil distribution and churning gear power losses of gearboxes by smoothed particle hydrodynamics. Proc Inst Mech Eng Part J J Eng Tribol 233(1):74–86

24. Liu H, Jurkschat T, Lohner T, Stahl K (2018) Detailed investigations on the oil flow in dip-lubricated gearboxes by the finite volume CFD method. Lubricants 6(2):47

25. Liu H, Jurkschat T, Lohner T, Stahl K (2017) Determination of oil distribution and churning power loss of gearboxes by finite volume CFD method. Tribol Int. https://doi.org/10.1016/j.triboint.2016.12.042

26. Liu H, Link F, Lohner T, Stahl K (2019) Computational fluid dynamics simulation of geared transmissions with injection lubrication. Proc Inst Mech Eng Part C J Mech Eng Sci 233(21–22):7412–7422

27. Liu H, Standl P, Sedlmair M, Lohner T, Stahl K (2018) Efficient CFD simulation model for a planetary gearbox. Forsch Ingenieurwes 82(4):319–330

28. Maccioni L, Concli F (2020) Computational fluid dynamics applied to lubricated mechanical components: review of the approaches to simulate gears, bearings, and pumps. Appl Sci 10(24):8810

29. Marchesse Y, Changenet C, Ville F (2019) Drag power loss investigation in cylindrical roller bearings using CFD approach. Tribol Trans 62(3):403–411

30. Mastrone MN, Hartono EA, Chernoray V, Concli F (2020) Oil distribution and churning losses of gearboxes: experimental and numerical analysis. Tribol Int 151(2):106496

31. Maurer J (1994) Lastunabhängige Verzahnungsverluste schnelllaufender Stirnradgetriebe. Dissertation, Universität Stuttgart, Stuttgart

32. Mauz W (1987) Hydraulische Verluste von Stirnradgetrieben bei Umlaufgeschwindigkeiten bis 60m/s. Dissertation, Universität Stuttgart, Stuttgart

33. Morhard B, Schweigert D, Mileti M, Sedlmair M, Lohner T, Stahl K (2020) Efficient lubrication of a high-speed electromechanical powertrain with holistic thermal managament. Forsch Ingenieurwes. https://doi.org/10.1007/s10010-020-00423-0

34. Neurouth A, Changenet C, Ville F, Octrue M, Tinguy E (2017) Experimental investigations to use splash lubrication for high-speed gears. J Tribol 139(6):61104

35. Norgauer P, Grunewald L, Priester L, Heilemann J, Hein M, Stahl K (2020) Experimentelle Ermittlung der Ölströmung in tauchgeschmierten Schneckengetrieben. Forsch Ingenieurwes 84(2):141–150

36. Oertel H, Böhle M, Reviol T (2015) Strömungsmechanik. Springer, Wiesbaden

37. Otto H-P (2009) Flank load carrying capacity and power loss reduction by minimised lubrication. Dissertation, Technische Universität München, München

38. Pallas S, Marchesse Y, Changenet C, Ville F, Velex P (2012) A windage power loss model based on CFD study about the volumetric flow rate expelled by spur gears. Mech Ind 13(5):317–323

39. Quiban R, Changenet C, Marchesse Y, Ville F (2021) Experimental investigations about the power loss transition between churning and windage for spur gears. J Tribol 143(2):205

40. Ruzek M, Marchesse Y, Ville F, Velex P (2019) Windage power loss reductions in high-speed gear pairs. Forsch Ingenieurwes 83(3):387–392

41. Schwarze R (2013) CFD-Modellierung. Springer, Berlin, Heidelberg, New York

42. Seetharaman S, Kahraman A (2009) Load-independent spin power losses of a spur gear pair: model formulation. Proc Inst Mech Eng Part J J Eng Tribol 131(2):22201

43. Seetharaman S, Kahraman A, Moorhead MD, Petry-Johnson TT (2009) Oil churning power losses of a gear pair: experiments and model validation. J Mech Des 131(2):151

44. Shadloo MS, Oger G, Le Touzé D (2016) Smoothed particle hydrodynamics method for fluid flows, towards industrial applications: motivations, current state, and challenges. Comput Fluids 136(1):11–34

45. Yakhot V, Smith LM (1992) The renormalization group, the ε-expansion and derivation of turbulence models. J Sci Comput 7(1):35–61